RSC Advances

ROYAL SOCIETY OF CHEMISTRY

www.rsc.org/advances

Journal Name

RSCPublishing

ARTICLE

Synthesis and electrochemical characteristics of $Li_{1.2}(Ni_{0.2}Mn_{0.6})_x(Co_{0.4}Mn_{0.4})_y(Ni_{0.4}Mn_{0.4})_{1-x-y}O_2$ ($0\leq x+y\leq 1$) cathode materials for lithium ion batteries

Cite this: DOI: 10.1039/x0xx00000x

Received 00th January 2012,
Accepted 00th January 2012

DOI: 10.1039/x0xx00000x

www.rsc.org/

Chao Zhang, Peiyu Hou , Xixi Shi*, Dawei Song, Jishun Song and Lianqi Zhang*

According to the tetrahedral phase diagram of $LiNiO_2$-$LiCoO_2$-$LiMnO_2$-Li_2MnO_3, a series of $Li_{1.2}(Ni_{0.2}Mn_{0.6})_x(Co_{0.4}Mn_{0.4})_y(Ni_{0.4}Mn_{0.4})_{1-x-y}O_2$ ($0\leq x+y\leq 1$) have been designed to explore new Li-rich solid solution cathode materials. The effects of $Li_{1.2}Ni_{0.2}Mn_{0.6}O_2$, $Li_{1.2}Co_{0.4}Mn_{0.4}O_2$ and $Li_{1.2}Ni_{0.4}Mn_{0.4}O_2$ content in solid solutions on structure and electrochemical property are investigated. Micro-sized spherical or ellipsoidal precursors are firstly prepared via a carbonate co-precipitation route. After calcination with lithium sources, all samples are indexed to a typical layered structure with an $R\bar{3}m$ space group as detected by X-ray diffraction (XRD). It is found that the introduction of Co can improve the tap density. However, these Co referred samples reveal lower discharge specific capacities and inferior cycle life. For these Co-free materials with high Ni content, for instance $Li_{1.2}Ni_{0.3}Mn_{0.5}O_2$, although low capacity is observed in initial cycle, large capacity of above 250 mAh g^{-1} is achieved after about 10 cycles. Importantly, the activated $Li_{1.2}Ni_{0.3}Mn_{0.5}O_2$ material still delivers a high capacity of over 230 mAh g^{-1} after 70 cycles, displaying superior cycle stability. These results may be instructive in designing and exploring high performance cathode materials for advanced LIBs.

1 Introduction

The depletion of traditional energy resources as well as the desire to reduce high CO_2 emissions associated with energy productions indicates that clean energy storage is now becoming more important than ever. Rechargeable lithium-ion batteries (LIBs) have become one of the key points of the development of clean energy, and its application range is keeping expanded. Since Sony announced the commercial availability of the rechargeable LIBs, layered $LiMO_2$ has been widely used as cathode materials[1,2].

Recently, much attention has focused on Li-rich layered materials as well as their related composite materials with spinel phases as cathode material for the next generation LIBs[3-31]. Li-rich layered materials usually show interesting electrochemical properties, such as large reversible capacity of over 250 mAh g^{-1} and excellent cycle life when cycled to an upper cutoff voltage of about 4.8 V. These materials can be generally expressed as formula $Li_{1+z}M_{1-z}O_2$ (M can be one or multi-metal ions, $z>0$)[25]. In our opinion, Li-rich layered ordered/disordered materials $Li_{1+z}M_{1-z}O_2$ can be all regarded as the $LiAO_2$-Li_2BO_3 solid solutions, which are based on the structure of rock salt; layered ordered structure can be further regarded as a solid solution material between layered $LiAO_2$ and Li_2BO_3[25]. Considering that the complexity in material composition and structure as well as valence variability is extremely easy to cause confusion on the reader to understand, we have proposed a tetrahedral phase diagram of $LiNiO_2$-$LiCoO_2$-$LiMnO_2$-Li_2MnO_3, as shown in Fig. 1, to describe and understand the nature of such materials[24,25].

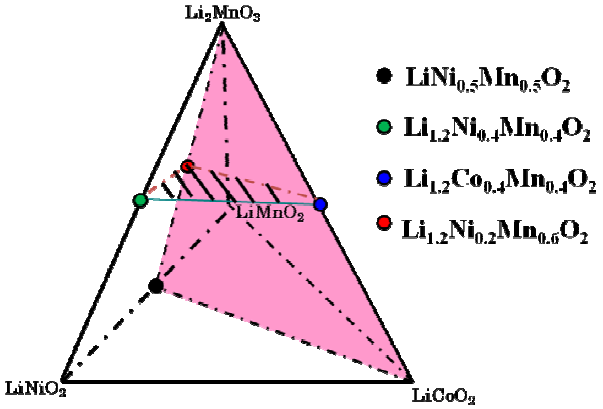

Fig. 1 The tetrahedral phase diagram of $LiNiO_2$-$LiCoO_2$-$LiMnO_2$-Li_2MnO_3.

According to the previous reports[5,7,8,13,26-28], it may be deduced that pure phased solid solutions can be formed in the space of $LiNiO_2$-$LiCoO_2$-$LiNi_{0.5}Mn_{0.5}O_2$-Li_2MnO_3 via a high temperature solid reaction[25]. In this work, in order to further support the point as well as explore new Li-rich solid solution materials, the aim of this paper is to synthesize a series of Li-rich layered materials with the nominal compositions of $Li_{1.2}(Ni_{0.2}Mn_{0.6})_x(Co_{0.4}Mn_{0.4})_y(Ni_{0.4}Mn_{0.4})_{1-x-y}O_2$ ($0\leq x+y\leq 1$), as better described in Fig. 2, and investigate the effects of $Li_{1.2}Ni_{0.2}Mn_{0.6}O_2$, $Li_{1.2}Co_{0.4}Mn_{0.4}O_2$ and $Li_{1.2}Ni_{0.4}Mn_{0.4}O_2$ content in solid solutions on structure and electrochemical properties.

Theoretically, such a substitution can be assumed on line 1 that one Ni^{3+} replaces one Mn^{4+}, accompanying oxidization of one Ni^{2+} to Ni^{3+} with decrease of x value. Similarly, on line 2 there exists a substitution equation (valence of $2Co^{3+}$ is equal to that of Ni^{2+} and Mn^{4+}, $Ni^{2+}+Mn^{4+}=2Co^{3+}$), and on line 3 Ni^{3+} is gradually substituted for Co^{3+} with the increase of y value. In addition, a carbonate co-precipitation route followed by a heat-treatment reaction is used to prepare monodisperse spherical particles.

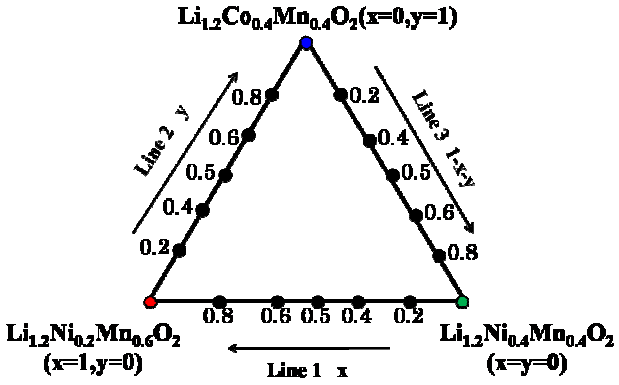

Fig. 2 The triangle phase diagram of $Li_{1.2}Ni_{0.2}Mn_{0.6}O_2$-$Li_{1.2}Co_{0.4}Mn_{0.4}O_2$-$Li_{1.2}Ni_{0.4}Mn_{0.4}O_2$. Any compositions in the diagram can be all express with x and y values, that is $Li_{1.2}(Ni_{0.2}Mn_{0.6})_x(Co_{0.4}Mn_{0.4})_y(Ni_{0.4}Mn_{0.4})_{1-x-y}O_2$ ($0\le x+y\le 1$).

2 Experimental

To synthesize the $(Ni_{0.25}Mn_{0.75})_x(Co_{0.5}Mn_{0.5})_y(Ni_{0.5}Mn_{0.5})_{1-x-y}CO_3$ ($0\le x+y\le 1$) carbonate precursors, stoichiometric $NiSO_4\cdot 6H_2O$, $CoSO_4\cdot 7H_2O$ and $MnSO_4\cdot H_2O$ were dissolved with a concentration of 2.0 mol L^{-1} as the starting materials. A mixed aqueous solution with 2.0 mol L^{-1} Na_2CO_3 and 0.2 mol L^{-1} NH_4OH (as the chelating agent) was also prepared as the starting alkali solution. The starting alkali and sulfates solutions were simultaneously pumped into a continuously stirred tank reactor (CSTR, capacity of 10 L) with 4 L water under a nitrogen atmosphere and reacted by controling pH value as 8.5, leading to the $(Ni_{0.25}Mn_{0.75})_x(Co_{0.5}Mn_{0.5})_y(Ni_{0.5}Mn_{0.5})_{1-x-y}CO_3$.

The obtained precursor powders were separated from the aqueous medium. After washed and filtered several times, they were dried inside a drying oven at 100 °C for 24 hours. Thereafter, stoichiometric amounts of Li_2CO_3 were well mixed with the carbonate precursors. The mixture was firstly calcined at 600 °C for 10 h to decompose the carbonate precursors and then calcined at 900 °C for 15 h to obtain the compounds.

Precursors were periodically collected during the co-precipitation experiment and the particle size distribution was measured by a particle size analyzer (OMEC, LS-POP(6), China). X-ray Diffractometry (XRD, Rigaku D/MAX -2500 Japan) was employed to characterize structure of the prepared materials. XRD data were obtained at 2θ=10°-80° with a step size of 0.02°, using Cu Kα radiation. The morphology of synthesized materials was observed by a Scanning Electron Microscope (SEM, JMS-6700F, JEOL, Japan). The tap density of materials was tested by ZS Tap Density (ZS-201).

For fabrication of cathode electrodes, the prepared materials were mixed with acetylene black and PVDF (80:10:10 in weight) in NMP. The obtained slurry was coated onto Al foil and dried at 80 °C for a day, followed by a roll-pressing. Prior to use, the electrodes were dried again at 120 °C for half a day in a vacuum oven. The electrodes were electrochemically characterized using a CR2032 type of coin cell with lithium foil as the anode and 1 M $LiPF_6$ in ethylene carbonate and diethyl carbonate (1:1 in volume) as the electrolyte. The cells were preliminarily charged and discharged in the voltage range of 2.0–4.8 V (versus Li) at 25 °C at a constant current density of 20 mA g^{-1}.

3 Results and discussion

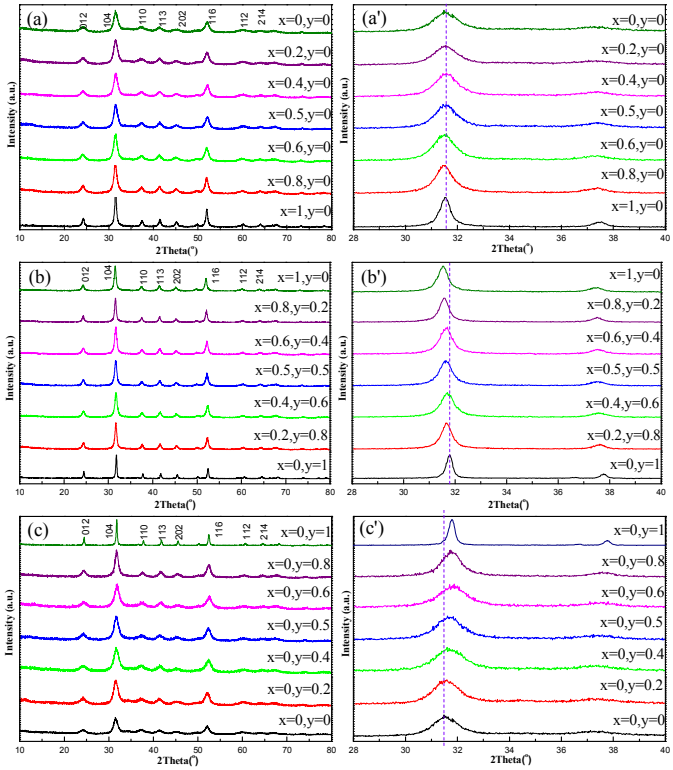

Fig. 3 XRD patterns of as-prepared carbonate precursors via a co-precipitation route. Full XRD patterns of samples on (a) line 1, (b) line 2 and (c) line 3, respectively. Local magnified XRD patterns near the (104) peak on (a') line 1, (b') line 2 and (c') line 3.

XRD patterns of as-prepared carbonate precursors $(Ni_{0.25}Mn_{0.75})_x(Co_{0.5}Mn_{0.5})_y(Ni_{0.5}Mn_{0.5})_{1-x-y}CO_3$ ($0\le x+y\le 1$) are revealed in Fig. 3. It can be seen that the precipitates are carbonate, because all reflections can be indexed to a space group of R-3c[29-31]. The regular shift in 2θ position can be found with careful observation, which can be clearly seen especially from Fig. 3(b') and 3(c'). These regular changes probly can result from the varation of transitional metals ion radius in $(Ni_{0.25}Mn_{0.75})_x(Co_{0.5}Mn_{0.5})_y(Ni_{0.5}Mn_{0.5})_{1-x-y}CO_3$. A similar discussion will be done in detail in XRD data of lithated compounds in Fig. 6. Therefore, the aimed carbonate precursors are successfully synthesized via the co-precipitation method in this work.

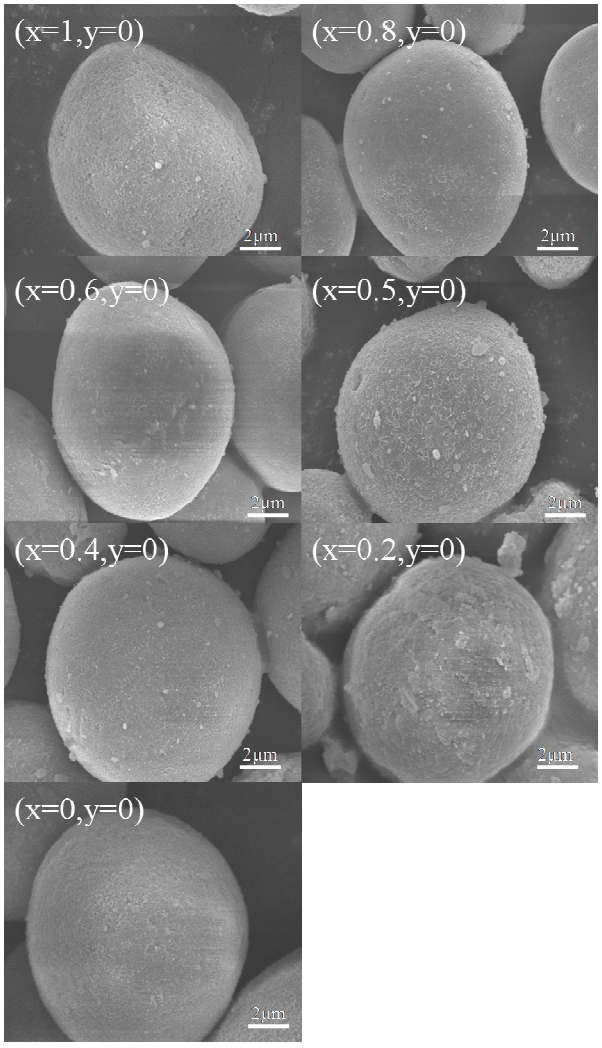

Fig. 4 The typical SEM images of as-prepared carbonate precursors: samples on line 1.

From the typical SEM images of carbonate precursors on line 1 (Fig. 4), all precursors have spherical or ellipsoidal secondary particles aggregated from nano-scaled primary particles. It is obvious that the smooth surface of the powders is achieved, meaning that primary particles are closely packed during co-precipitation. All samples have monodisperse particles, suggesting excellent flowability of material. The particle size distributions of carbonate precursors are analyzed and the results are shown in Fig. 5. Clearly, all precursors have a single and normal distribution, but particle size seems to depend somewhat on the component[29-31]. We believe that the nucleus formation and crystal growth highly depends on the reaction conditions in CSRT and the ratio of Ni/Co/Mn. In our work, the high Ni element appears to hinder the growth of precursors, which is probably attributed to the lower K_{sp} of $NiCO_3$ compared with that of $CoCO_3$ and $MnCO_3$.

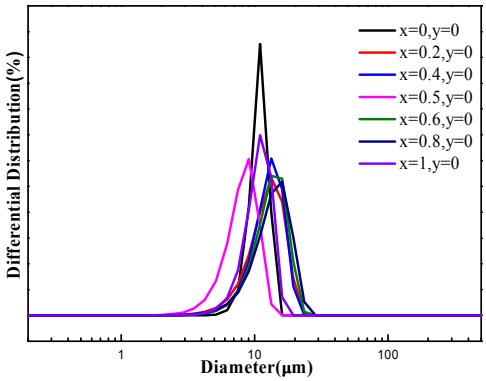

Fig. 5 Particle size distribution curves of as-prepared carbonate precursors on line 1.

The micro-spherical powders have close packing and monodisperse performances, and thus high tap density can be anticipated for as-prepared precursors. The detailed tap densities are listed in Table 1, in which the tap densities of $Ni_{0.25+x}Mn_{0.75-x}CO_3$ ($0 \le x \le 0.2$) compositions on line 1 remain around 1.60 g cm^{-3} even increasing Ni content. Interestingly, an increased tap density presents as Co content ranges from 0 to 0.4 on line 2. It is concluded that the tap density is related to the content of Co in carbonate precursors $Ni_xCo_yMn_{1-x-y}CO_3$. The similar results is also observed on line 3. These results provide a new insight to explore high volumetric energy density cathode materials for advanced LIBs.

Table 1 Tap densities of as-prepared carbonate precursors.

Samples	Tap density (g cm^{-3})	Samples	Tap density (g cm^{-3})	Samples	Tap density (g cm^{-3})
x=0,y=0	1.65	x=1,y=0	1.59	x=0,y=1	1.80
x=0.2,y=0	1.56	x=0.8,y=0.2	1.62	x=0,y=0.8	1.77
x=0.4,y=0	1.62	x=0.6,y=0.4	1.66	x=0,y=0.6	1.75
x=0.5,y=0	1.59	x=0.5,y=0.5	1.69	x=0,y=0.5	1.73
x=0.6,y=0	1.63	x=0.4,y=0.6	1.73	x=0,y=0.4	1.72
x=0.8,y=0	1.61	x=0.2,y=0.8	1.77	x=0,y=0.2	1.69
x=1,y=0	1.59	x=0,y=1	1.80	x=0,y=0	1.65

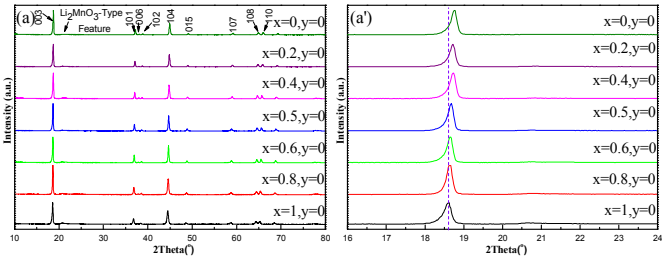

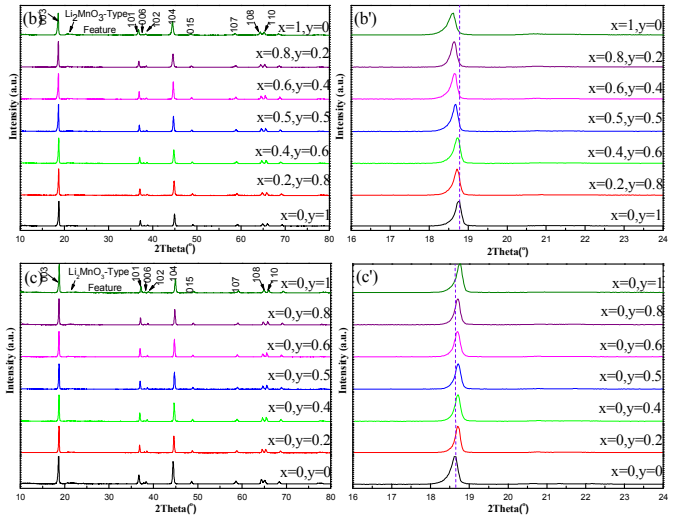

Fig. 6 XRD patterns of $Li_{1.2}(Ni_{0.2}Mn_{0.6})_x(Co_{0.4}Mn_{0.4})_y(Ni_{0.4}Mn_{0.4})_{1-x-y}O_2$ ($0\le x+y\le 1$). Full XRD patterns of samples on (a) line 1, (b) line 2 and (c) line 3, respectively. Local magnified XRD patterns near the (003) peak on (a') line 1, (b') line 2 and (c') line 3.

XRD patterns of $Li_{1.2}(Ni_{0.2}Mn_{0.6})_x(Co_{0.4}Mn_{0.4})_y(Ni_{0.4}Mn_{0.4})_{1-x-y}O_2$ ($0\le x+y\le 1$) are displayed in Fig. 6. As shown in Fig. 6(a), (b) and (c), all the strong diffraction peaks of oxides could be indexed to a well-defined hexagonal α-$NaFeO_2$-type structure with a space group of $R\bar{3}m$. The additional weak reflections at around 2θ=20–25° can be attributed to the short-ranged superlattice due to the ordering of Li, Ni, Co, and Mn cations in the transition metal layers[3,4,7-9,17,18]. Furthermore, the clear split between the adjacent peaks of (006)/(102) and (018)/(110) suggests a well-developed layered structure for all samples. The lattice parameters of all oxides are calculated, as displayed in Fig. 7. For the samples of line 1, a roughly linear increase in lattice parameters, a and c, can be seen with increase of x value, which may be associated with the change in average ions radius of transitional metals. In line 1, there is substitution equation of $2Ni^{3+}=Ni^{2+}+Mn^{4+}$. The average ion radius of Ni^{2+} and Mn^{4+} is 0.615 Å (the ion radii of Ni^{2+} and Mn^{4+} are 0.69 and 0.54 Å, respectively) while the radius of Ni^{3+} is 0.56 Å[32]. Therefore, a larger average ion radius with increasing x value should be responsible for the gradual increase in lattice parameters. On line 2, lattice parameters by contrast linearly decreases with increasing Co content, which can be also explained by the change in average ion radius of transitional metals. As assumed in the introduction, such a substitution equation as $Ni^{2+}+Mn^{4+}=2Co^{3+}$ exists in line 2. The ion radius of Co^{3+} (0.53 Å) is smaller than the average one of $Ni^{2+}$and Mn^{4+} (0.615 Å) [32]. In line 3, a linear increase in lattice parameters with increasing y value is observed, which may be also ascribed to a larger Ni^{3+} in contrast to Co^{3+}. The linear change in lattice parameter in turn also supports the formation of solid solution among three compounds of $Li_{1.2}Ni_{0.2}Mn_{0.6}O_2$, $Li_{1.2}Co_{0.4}Mn_{0.4}O_2$ and $Li_{1.2}Ni_{0.4}Mn_{0.4}O_2$.

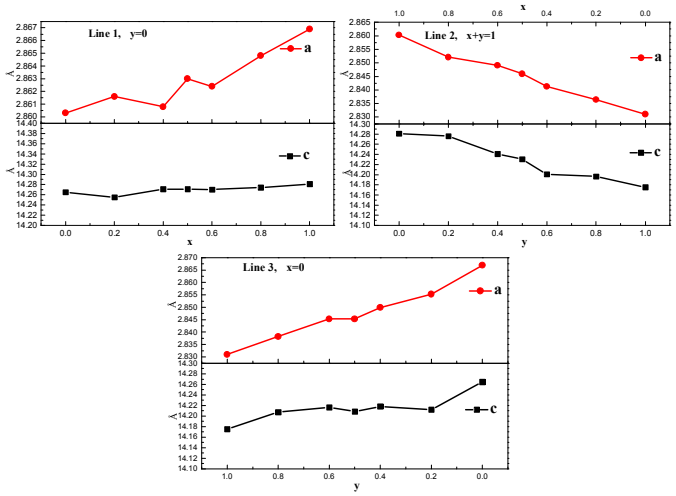

Fig. 7 The lattice parameters of $Li_{1.2}(Ni_{0.2}Mn_{0.6})_x(Co_{0.4}Mn_{0.4})_y(Ni_{0.4}Mn_{0.4})_{1-x-y}O_2$ ($0\le x+y\le 1$).

SEM images of $Li_{1.2}(Ni_{0.2}Mn_{0.6})_x(Co_{0.4}Mn_{0.4})_y(Ni_{0.4}Mn_{0.4})_{1-x-y}O_2$ ($0\le x+y\le 1$) are showed in Fig. 8. Clearly, spherical or ellipsoidal morphologies of secondary particles are remained for these solid solution materials even after being re-crystallized with lithium sources during high temperature calcination process. Spherical cathode materials have many advantages such as higher packing density and smaller specific surface area, which then enhances volumetric energy density and reduces side reactions between cathode particle and electrolyte. After lithiation, several hundreds nanosized primary particles are revealed in Fig. 8. Meanwhile, the introduction of Co seems to cause porous structure. Usaully, the primary particle size and surface morphology play important roles in physical and electrochemical properties such as electrolyte wetting, surface resistance, rate properties and tap density[29-31].

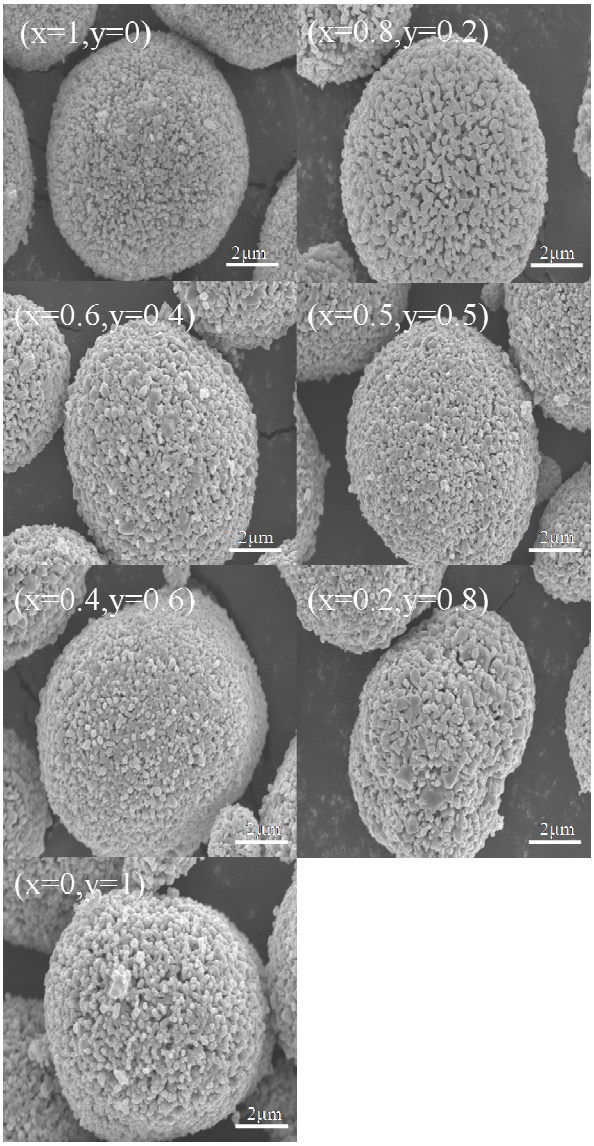

Fig. 8 The typical SEM images of $Li_{1.2}(Ni_{0.2}Mn_{0.6})_x(Co_{0.4}Mn_{0.4})_y(Ni_{0.4}Mn_{0.4})_{1-x-y}O_2$ ($0\le x+y\le 1$): samples on line 2

Table 2 Tap densities of $Li_{1.2}(Ni_{0.2}Mn_{0.6})_x(Co_{0.4}Mn_{0.4})_y(Ni_{0.4}Mn_{0.4})_{1-x-y}O_2$ ($0\le x+y\le 1$).

Samples	Tap density (g cm^{-3})	Samples	Tap density (g cm^{-3})	Samples	Tap density (g cm^{-3})
x=0,y=0	2.07	x=1,y=0	1.98	x=0,y=1	2.12
x=0.2,y=0	1.95	x=0.8,y=0.2	2.00	x=0,y=0.8	2.11
x=0.4,y=0	2.01	x=0.6,y=0.4	2.03	x=0,y=0.6	2.09
x=0.5,y=0	1.97	x=0.5,y=0.5	2.05	x=0,y=0.5	2.09
x=0.6,y=0	2.01	x=0.4,y=0.6	2.07	x=0,y=0.4	2.07
x=0.8,y=0	1.99	x=0.2,y=0.8	2.09	x=0,y=0.2	2.07
x=1,y=0	1.98	x=0,y=1	2.12	x=0,y=0	2.07

Volumetric energy density, which is highly related on tap density, is a key factor in Li-ion battery system. The tap densities of $Li_{1.2}(Ni_{0.2}Mn_{0.6})_x(Co_{0.4}Mn_{0.4})_y(Ni_{0.4}Mn_{0.4})_{1-x-y}O_2$ ($0\le x+y\le 1$) are listed in Table 2. The samples on line 1 show similar tap density of about 2.0 g cm^{-3}. An increased tap density is achieved while enhancing the Co content, and $Li_{1.2}Co_{0.4}Mn_{0.4}O_2$ delivers the highest tap density of 2.12 g cm^{-3}.

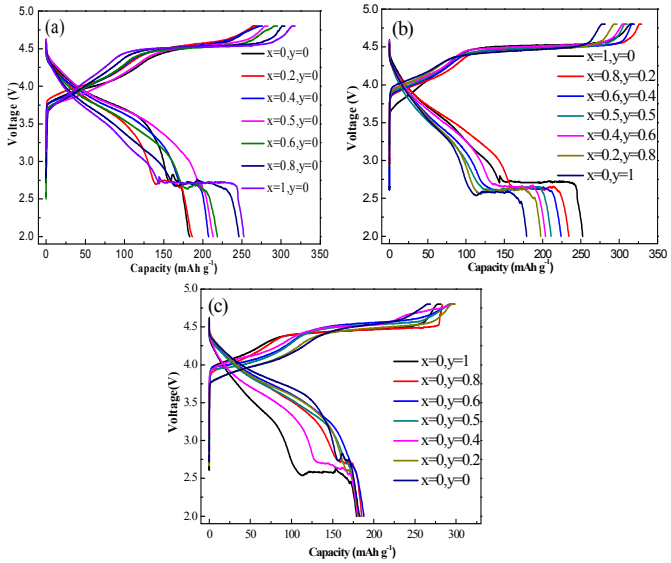

Fig. 9 The initial charge-discharge curves of $Li_{1.2}(Ni_{0.2}Mn_{0.6})_x(Co_{0.4}Mn_{0.4})_y(Ni_{0.4}Mn_{0.4})_{1-x-y}O_2$ ($0\le x+y\le 1$): (a) samples of line 1, (b) samples of line 2, (c) samples of line 3.

Fig. 9 shows the initial charge-discharge curves of $Li_{1.2}(Ni_{0.2}Mn_{0.6})_x(Co_{0.4}Mn_{0.4})_y(Ni_{0.4}Mn_{0.4})_{1-x-y}O_2$ ($0\le x+y\le 1$) in the voltage range of 2.0–4.8 V at a current density of 20 mA g^{-1}. The initial charge-discharge capacities and coulombic efficiencies of these samples are summarized in Table 3. The charge capacity below 4.5 V is usually attributed to the oxidation of Ni^{2+}/ Ni^{3+} to Ni^{4+} and Co^{3+} to Co^{4+} while the initial plateau region at around 4.5V is correlated with the simultaneous expulsion of oxygen and Li^+ [4,11,13,17]. In Fig. 9(a), with the increase of x value the capacity below 4.5V gradually decreases, but the initial charge plateau gradually prolongs, finally indicating gradually increased initial charge capacity. This implies that the samples with Ni^{2+} are possibly easier to present the reaction of the simultaneous expulsion of oxygen and Li^+ than that with Ni^{3+}. At the same time, the discharge capacity also gradually increase with increasing x. However, a discharge plateau at around 2.7 V is observed and gradually becomes long with increasing x. For Li-rich layered material, origin of the voltage plateau at around 2.7 V for the first discharge process was discussed and verified in a recent report[17]. It has been proposed that the oxygen molecule generated in the initial charge process at the high voltage plateau is electrochemically reduced with one electron reduction process below 3.0 V during the subsequent discharge process, forming a superoxide, Li_2O_2[17]. The discharge plateau is also similar to that observed in Li-O_2 battery system[33,34]. In fact, in some early reports[12,24,28], the discharge plateau at around 2.7 V during initial discharge process could be also seen

with careful observation and analysis for some Li-rich materials. In this work, the phenomenon become apparent for some samples, which may be possibly associated with such factors as the samples prepared via a co-precipitation of carbonate as well as characterization of electrochemical properties using coin cell method with small amounts of electrolyte. In addition, another abnormal phenomenon is that the jumping of voltage at the plateau of around 2.7 V is observed for some samples. Repeated experiments and using other commercial electrolyte in our lab still cannot eliminate the phenomenon. It is unclear for us at present. Probably, it is associated with the process of ineffective reduction of oxygen.

As to the materials in line 2, the charge capacities are alike and about 105 mAh g^{-1} under 4.5 V. Long plateau regions and charge capacities of above 200 mAh g^{-1} are revealed between 4.5–4.8 V in Fig. 9(b). Nevertheless, the discharge capacity below 3.0 V decreases with the increase of Co^{3+} content. Compared to these samples in line 1 and 2, the samples in line 3 have shorter plateaus above 4.5 V and lower initial charge-discharge capacities, as shown in Fig. 9(c) and Table 3.

Table 3 Initial charge-discharge capacities and coulombic efficiencies of $Li_{1.2}(Ni_{0.2}Mn_{0.6})_x(Co_{0.4}Mn_{0.4})_y(Ni_{0.4}Mn_{0.4})_{1-x-y}O_2$ ($0\le x+y\le 1$).

Samples	Initial charge capacities (mAh g^{-1})	Initial discharge capacities (mAh g^{-1})	Coulombic efficiencies (%)
x=0,y=0	268.9	183.1	68.1
x=0.2,y=0	270.8	186.5	68.9
x=0.4,y=0	276.1	207.4	75.1
x=0.5,y=0	283.1	213.1	75.3
x=0.6,y=0	295.4	218.7	74.0
x=0.8,y=0	304.9	246.7	80.7
x=1,y=0	318.0	252.4	79.4
x=0.8,y=0.2	329.2	234.1	71.1
x=0.6,y=0.4	319.6	224.1	70.1
x=0.5,y=0.5	310.3	211.0	68.0
x=0.4,y=0.6	307.7	203.7	66.2
x=0.2,y=0.8	297.1	197.6	66.5
x=0,y=1	281.5	179.1	63.6
x=0,y=0.8	283.6	185.3	65.3
x=0,y=0.6	295.9	188.1	63.6
x=0,y=0.5	297.7	181.8	61.1
x=0,y=0.4	298.5	180.1	60.3
x=0,y=0.2	298.8	181.7	60.8
x=0,y=0	268.9	183.1	68.1

Fig. 10 shows the cycle performances of $Li_{1.2}(Ni_{0.2}Mn_{0.6})_x(Co_{0.4}Mn_{0.4})_y(Ni_{0.4}Mn_{0.4})_{1-x-y}O_2$ ($0\le x+y\le 1$) in the voltage rang of 2.0–4.8 V at a current density of 20 mA g^{-1}. The samples on line 1 display superior cycle stability than samples on line 2 and 3. In Fig. 10(a), the sample with x=0.4 delivers the stable and highest discharge capacity of more than 250 mAh g^{-1} after initial several cycles. The discharge capacity intends to decrease with a higher Ni content. From Fig. 10(b), it can be concluded that the introduction of Co leads inferior cycling life and lower discharge capacity. Fig. 10(c) also displays that the replacement of Co^{3+} by Ni^{3+} can enhance the cycle stability.

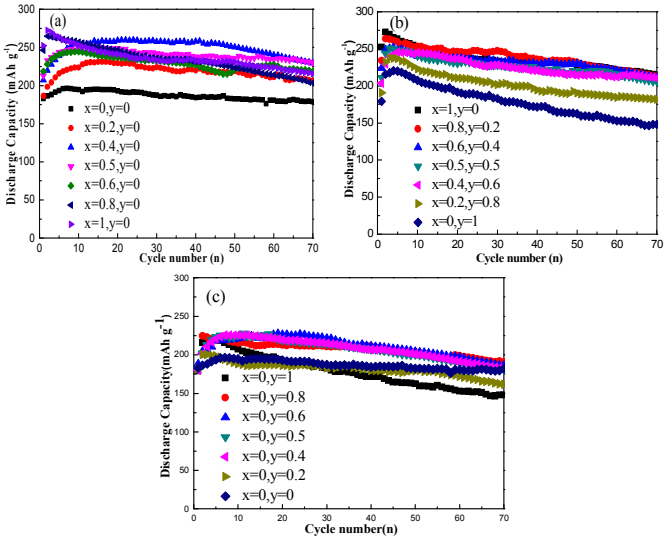

Fig. 10 Cycle performances of $Li_{1.2}(Ni_{0.2}Mn_{0.6})_x(Co_{0.4}Mn_{0.4})_y(Ni_{0.4}Mn_{0.4})_{1-x-y}O_2$ ($0\le x+y\le 1$): (a) samples of line 1, (b) samples of line 2, (c) samples of line 3.

4 Conclusions

A series of layered oxides $Li_{1.2}(Ni_{0.2}Mn_{0.6})_x(Co_{0.4}Mn_{0.4})_y(Ni_{0.4}Mn_{0.4})_{1-x-y}O_2$ ($0\le x+y\le 1$) have been designed to explore new Li-rich solid solution cathode materials on the basis of tetrahedral phase diagram of $LiNiO_2$-$LiCoO_2$-$LiMnO_2$-Li_2MnO_3. Micro-sized spherical or ellipsoidal precursors were successfully prepared via a carbonate co-precipitation route. After calcination with lithium sources, the solid solution materials were obtained and all samples can be indexed to a typical layered structure with a $R\bar{3}m$ space group. The introduction of Co can efficiently improve the tap density of solid solution materials. However, these Co referred samples have lower discharge capacities and suffer from low capacity retention during long cycle.

Eletrochmical performances closely depend on material compoisitions. Among these solid solution materials, $Li_{1.2}Ni_{0.3}Mn_{0.5}O_2$ can deliver a high discharge capacity more than 250 mAh g^{-1} after initial 10 cycles, although a relatively low capacity is observed in initial cycle. More importantly, the activated $Li_{1.2}Ni_{0.3}Mn_{0.5}O_2$ material delivers high discharge capacity of over 230 mAh g^{-1} even after 70 cycles, indicating superior cycle stability in the range of 2.0–4.8 V. In addition, the apparent reduction of oxygen marked as a discharge plateau at around 2.7 V during the initial discharge process is observed clearly in our work. Thus these results may provide a new insight into explore high-performance cathode materials for advanced LIBs.

Acknowledgements

This work was financially supported by National 863 Program of China (2013AA050906), NSFC (51272175, 21301127).

Notes and references

School of Materials Science and Engineering, Tianjin University of Technology, Tianjin 300384, China. E-mail: tianjinzhanglq@163.com; cshi6@163.com; Fax: +86 22 60214028; Tel: +86 22 60214577.

1 V. Etacheri, R. Marom, R. Elazari, G. Salitra, D. Aurbach, *Energy Environ. Sci.,* 2011, **4**, 3243.
2 S.S. Jan, S. Nurgul, X. Shi, H. Xia, H. Pang, *Electrochem. Acta*, 2014, **149**, 86.
3 Z. Lu, D.D. MacNeil, J.R. Dahn, *Electrochem. Solid-State Lett.,* 2001, **4,** A191.
4 Z. Lu, J.R. Dahn, *J. Electrochem. Soc.,* 2002, **149,** A815.
5 L.Q. Zhang, K. Takada, N. Ohta, L.Z. Wang, T. Sasaki, M. Watanabe, *Mater. Lett.*, 2004, **58**, 3197.
6 J.S. Kim, C.S. Johnson, J.T. Vaughey, M.M. Thackeray, S.A. Hackney, W. Yoon, C.P. Gray, *Chem. Mater.,* 2004, **16,** 1996
7 L.Q. Zhang, K. Takada, N. Ohta, K. Fukuda, M. Osada, L.Z. Wang, T. Sasaki, M. Watanabe, *J. Electochem. Soc.*, 2005, **152**, A171.
8 J. Jiang, K.W. Eberman, L.J. Krause, J.R. Dahn, *J. Electochem. Soc.*, 2005, **152**, A1879.
9 J. Jiang, J.R. Dahn, *Electrochim. Acta*, 2006, **51**, 3413.
10 Y. Sun, Y. Xia,Y. Shiosaki, H. Noguchi, *Electrochim. Acta*, 2006, **51**, 5581.
11 A.R. Armstrong, P. Holzapfel, P. Novak, C.S. Johnson, S.H. Kang, M.M. Thackeray, P.G. Bruce, *J. Am. Chem. Soc.* 2006, **128,** 8694.
12 J.M. Kim, S. Tsuruta, N. Kumagai, *Electrochem. Commun.*, 2007, **9**, 103.
13 T. A. Arunkumar, Y. Wu, A. Manthiram, *Chem. Mater.* 2007, **19**, 3067.
14 C.S. Johnson, N. Li, C. Lefief, J.T. Vaughey, M.M. Thackeray, *Chem. Mater.*, 2008, **20**, 6095.
15 J.M. Zheng, Z.R. Zhang, X.B. Xu, Z.X. Dong, Z. Zhu, Y. Yang, *J. Electrochem. Soc.*, 2008, **155**, A775.
16 I. Atsushi, D.C. Li , Y. Sato, *J. Power Sources*, 2010, **195**, 567.
17 N. Yabuuchi, K. Yoshii, S.T. Myung, I. Nakai, S. Komaba, *J. Am. Chem. Soc.*, 2011, **133**, 4404.
18 K.A. Jarvis, Z.Q. Deng, L.F. Allard, A. Manthiram, P.J. Ferreira, *Chem. Mater.*, 2011, **23**, 3614.
19 J. Bareno, M. Balasubramanian, S.H. Kang, J.G. Wen, C.H. Lei, V. Pol, I. Petrov, D.P. Abraham, *Chem. Mater*. 2011, **23**, 2039.
20 L. Li , Y.L. Chang, H. Xia, B.H. Song, J.R. Yang, K.S. Lee, L. Lua, *Solid State Ionics*, 2014, **264**, 36.
21 X. Huang, M. Wang, R. Che, *J. Mater. Chem.*, 2014, **2**, 9656.
22 J. Ma, Y. N. Zhou, Y. Gao, Q. Kong, Z. Wang, X. Q. Yang, L. Chen, *Chem. Eur. J.*, 2014, **20**, 8723.
23 J. Lu, Y. Chang, B. Song, H. Xia, J. Yang, K.S. Lee, L. Lu, *J. Power Sources*, 2014, **271**, 604.
24 L.Q. Zhang, Q.W. Peng, Z.W. Lu, L.B. Ren, H.Q. Ren, X.J. Liu, The 15th International Meeting on Lithum Batteries, Abstract #629, 2010, June 27-July 3 , Montreal, Canada.
25 L.Q. Zhang, C.W. Xiao, R.J. Yang, *Prog. in Chem.*, 2011, **23**, 410.
26 P.S. Whitfield, S. Niketic, I.D. Davidson, *J. Power Sources,* 2005, **146**, 617.
27 L.Q. Zhang, X.Q. Wang, T. Muta, D.C Li, H. Noguchi, M. Yoshio, R.Z. Ma, K. Takada, T. Sasaki, *J. Power Sources*, 2006, **162**, 629.
28 L.Q. Zhang, H. Noguchi, D.C. Li, T. Muta, X.Q. Wang, M. Yoshio, I. Taniguchi, *J. Power Sources*, 2008, **185**, 534.
29 D.K. Lee , S.H. Park , K. Amine, *J. Power Sources*, 2006, **162**, 1346.
30 H. Deng, I. Belharouak, R.E. Cook, H. Wu, Y.K. Sun, K. Amine, *J. Electrochem. Soc.*, 2010, **157**, A447.
31 D.P. Wang, I. Belharouak, G. M. Koenig, G. Zhou, K. Amine, *J. Mater. Chem.*, 2011, **21**, 9290.
32 R.D. Shannon, *Acta Crystallogr.,* 1976, A**32,** 751.
33 Z. Peng, S. A. Freunberger, Y. Chen, P. G. Bruce, *Science*, 2012, **337**, 563.
34 Z. Peng, S. A. Freunberger, L. J. Hardwick, Y. Chen, V. Giordani, F. Bardé, P. Novák, D. Graham, J.M. Tarascon, P. G. Bruce, *Angew. Chem. Int.*, 2011, **50**, 6351.